ACS APPLIED MATERIALS & INTERFACES

Research Article

www.acsami.org

Regioselective Patterning of Multiple SAMs and Applications in Surface-Guided Smart Microfluidics

Chuanzhao Chen,[‡] Pengcheng Xu,[‡] and Xinxin Li*[,‡]

State Key Lab of Transducer Technology, and, Science Technology on Micro-system Lab, Shanghai Institute of Micro-system and Information Technology, Chinese Academy of Sciences, 865 Changning Road, Shanghai 200050, China

Supporting Information

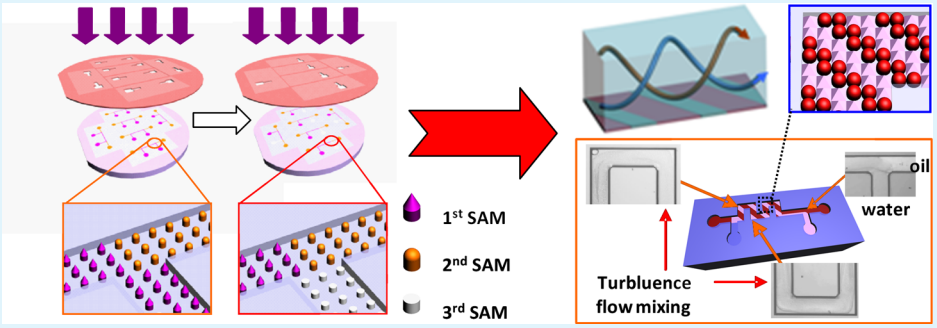

ABSTRACT: A top-down nanofabrication technology is developed to integrate multiple SAMs (self-assembled monolayers) into regioselective patterns. With ultraviolet light exposure through regioselectively hollowed hard mask, an existing SAM at designated microregions can be removed and a dissimilar kind of SAM can be regrown there. By repeating the photolithography-like process cycle, diverse kinds of SAM building blocks can be laid out as a desired pattern in one microfluidic channel. In order to ensure high quality of the surface modifications, the SAMs are vapor-phase deposited before the channel is closed by a bonding process. For the first time the technique makes it possible to integrate three or more kinds of SAMs in one microchannel. The technique is very useful for multiplex surface functionalization of microfluidic chips where different segments of a microfluidic channel need to be individually modified with different SAMs or into arrayed pattern for surface-guided fluidic properties like hydrophobicity/philicity and/or oleophobicity/philicity, etc. The technique has been well validated by experimental demonstration of various surface-directed flow-guiding functions. By modifying a microchannel surface into an arrayed pattern of multi-SAM "two-tone" stripe array, surface-guiding-induced 3D swirling flow is generated in a microfluidic channel that experimentally exhibits quick oil/water mixing and high-efficiency oil-to-water chemical extraction.

KEYWORDS: *passive mixing extraction, self-assembled monolayer, batch nanofabrication, integration of multiple SAMs, surface guide microfluidics, 3D swirling flow*

INTRODUCTION

A microfluidics-based micrototal analysis system (μ-TAS) has been intensively explored for biological/chemical analysis and medical detection. In a microchannel fluidic chip, guidance and operation of the fluid play key roles in rapid and precise analytical functions. In passive microchannels, surface modification can significantly improve fluidic properties or even realize some smart functions by surface-directed flow guidance. Compared to the methods of top-down microfabricating 3D microstructures,[1] bottom-up surface functionalization[2] has attracted more attention in recent years. Bottom-up construction does not need to change the channel geometries and influences less the fluidics. In addition, bottom-up surface modification can provide various flow resistances for control of microfluids by modifying surface molecule layers to adjust the interfacial energy at the solid/fluidics interface.

A self-assembled monolayer (SAM)[3,4] is a convenient bottom-up method for surface modification, which can build various surface functionalizations or provide a new interface for further graft of multilayer nanostructures. For example, SAM modification can realize surface functions such as adsorption/adhesion,[5,6] tunable wettability [hydro(oleo)philicity and/or hydro(oleo)phobicity],[7] corrosion prevention,[8] lubrication,[9] modification of electronic properties,[10] separation/mixing, and specific molecule interactions.[11] Via covalent bonding to the surface of silicon or glass substrate, silane SAM[12] is very stable and can be considered as a good candidate for desired fluidic surface functionalizations. In order to grow dense silane SAM, substrate material is required to be precovered by dense hydroxyl groups. After surface pretreatment, hydroxyl groups can be densely covered on the surface of silicon or glass for modification of silane SAM. Besides, silicon or glass material is

Received: June 24, 2014
Accepted: December 1, 2014
Published: December 1, 2014

quite stable under general chemistry operation with both aqueous and organic solvents.

Injecting liquid/vapor to coat a thin film[13] at desired parts of the microchannel surface is a commonly used method for fabricating surface-directed fluidic chips. Unfortunately, such kind of method is not applicable for batch fabrication and is not capable for formation of complexly patterned surface. By the aid of ultraviolet (UV) light,[14] regional liquid-phase modification is an elegant approach, which can meet the requirements of complex design and batch fabrication. However, the liquid-phase surface modification[2] is difficult to secure high uniformity of the modified thin film especially when the modification is implemented in a big-size wafer level. Aggregation of functional molecules easily leads to a clogging problem in very thin micro/nanochannels. L. Derzsi et al. tried to use a kind of hydrophobic material and UV light to form hydrophobic/hydrophilic pattern in fluidic channels.[15] Compared to the liquid-phase methods, this is a clean method and there is no need to remove the liquid residue in the channels. Unfortunately, the high surface energy created by UV exposure is instable and the hydrophilic surface will fade and change back to hydrophobic surface after several days. The problem may be solved by fabricating micro/nanochannels with native hydrophilic materials, e.g., silicon oxide or multifunctional acrylates.[16] In addition, the above-mentioned two methods[4,5] can only form two kinds of surface, i.e., modified/nonmodified or with/without nanomaterial coated. In the work by Shirai et al.,[17] APTES SAM was first deposited in the vapor phase and patterned using UV light. In this way both pattern formation and surface activation (for bonding) can be achieved simultaneously. After the channel was closed by a bonding process, PEG SAM was then modified in the liquid phase by injecting the fluid into the closed channel. With the liquid-phase modification for a closed channel, two kinds of SAMs were integrated.

In many microfluidic systems, three or more kinds of surface functions need to be integrated individually at different microregions of the fluidic channel. In the widely used μTAS,[18,19] surface effects play very important roles. In a smart microfluidic system, hydrophobicity/philicity, oelophobicity/philicity, and biochemical-specific affinities may be individually desired to be constructed at individual regions of the system. The performance of microfluid manipulation is highly dependent on the quality of surface function. Chemical vapor-phase deposition is a good method to obtain SAMs with high uniformity and high density. By the aid of deep UV light, three or more kinds of SAMs are expected to be integrated in an open microchannel before it is closed by a bonding process.

In this study, with the help of deep UV light (with a wavelength of 185−254 nm) and prepatterned hollow mask, the SAMs can be sequentially formed in different segments of a microchannel. The SAMs are vapor-phase deposited to ensure the quality of surface modification. An appropriate deposition sequence is needed to eliminate the interaction between different kinds of SAMs. Compared with a traditional quartz mask, the hollow mask helps to enhance the photochemical reaction rate for multi-SAMs patterning. With the method three or more kinds of SAMs can be sequentially grown at different microregions of a fluidic channel for individual functions, and similarly, a great number of such chips can be simultaneously fabricated at a big-size wafer level, is schematically shown in Figure 1. By analogy, many such big-sized wafers can be volume produced.

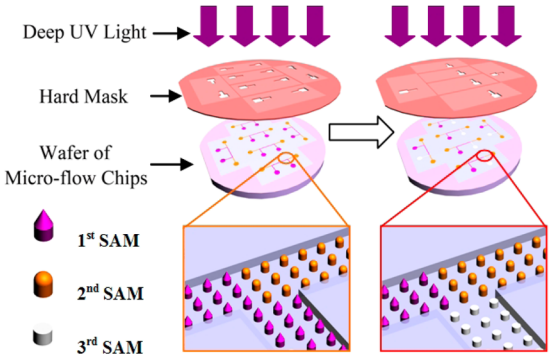

Figure 1. Schematic of wafer-level regioselective modifications. By repeatedly employing top-down batch-fabricating cycles of masked UV photolithography, multiple SAMs can be integrated on chips at the wafer level.

To validate the technique in microfluidic systems, various surface-directed flow-guiding functions have been experimentally demonstrated. By modifying the microchannel surface into a densely patterned oleophobic/oleophilic alternate stripe array, chaotic-flow enhanced oil/water mixing effect and highly efficient oil-to-water chemical extraction are successfully realized.

EXPERIMENTAL SECTION

SAM Growth by MVD. Surface modification of SAM is implemented using a MVD machine (MVD-100E, purchased from Applied Micro Structure Inc.). Under 0.05 Torr vacuum and 50 °C, the SAM layer is firmly self-assembled on a silicon surface by the aid of the catalytic agent of vaporized deionized water. All SAM precursor solutions used in this article are purchased from Gelest Inc. Prior to the deposition process, the SAM precursor is degassed in vacuum. After deposition, the silicon wafer is annealed in the chamber at 80 °C for 1 h.

SAM Patterning by O_3 Aided UV Exposure under Hard Mask. Photolithographic nanosurface patterning is performed at 100 °C for 30 min using a commercial deep UV cleaning system (PSD-UV, Novascan Technologies, Ames, IA) during which a distance of 4.0 cm is maintained between the channel surface and the UV lamp. Exposure of deep UV light (wavelength = 185−254 nm) on natural oxygen in air generates ozone to locally remove existing SAM. After the UV irradiation to remove existing siloxane-SAM on silicon wafer, an −OH-covered wetting surface will be formed for regrowth of another kind of SAM. The process principle is shown in Figure 2a and is discussed in the Results and Discussion.

Integration of Patterned Multi-SAMs in Microflow Channel. Schematically shown in Figure 2b is a typical example for patterning multiple surface functionalizations in a microchannel chip. The process steps are described as follows. (I) A 0.5 μm thick SiO_2 layer is thermally grown on a (100) silicon wafer and patterned as a mask using photoresist coating and wet HF etching. Then the wafer is immersed in 40% aqueous KOH at 50 °C to form the microflow channels by anisotropic etching. (II) To avoid SAM growth at undesired regions, a Cr/Au metal layer of 30 nm/60 nm in thickness is sputtered and patterned to cover the regions outside the channels. (III) The first layer of SAM, herein hydro/oleophobic FAS-17, is self-assembled with the MVD machine. (IV) This first SAM layer is patterned using a UV-photolithography-like step[20,21] under the first piece of silicon hard mask. The first SAM remains at the desired regions, while the SAM at other regions is removed by deep UV exposure. UV illumination can oxidize O_2 (in nature lab air) into ozone that further reacts with the $-CH_2-$ of the SAM molecule chain. (V) The second-layer SAM, herein oleophilic/hydrophobic OTS, is MVD self-assembled on the newly exposed regions. (VI) The third-layer SAM, herein hydro(oleo)philic silanol-SAM (by modifying −OH

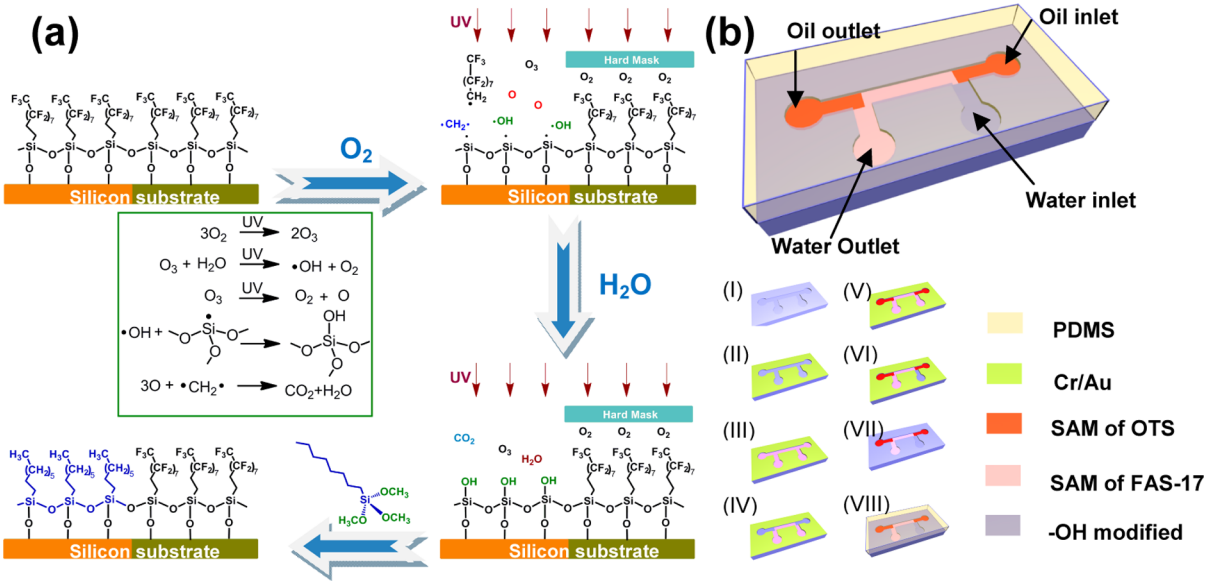

Figure 2. Schematic process-route for regioselective removal and alternative regrowth of SAMs. (a) Process cycle of removing the first siloxane SAM (herein exampled with FAS-17) and regrowing the second SAM (OTS as example) at the same area, which is based on UV photochemical reaction and self-assembly of siloxane SAM. (b) The processes are used for integration of regioselectively modified branches into a microchannel chip, where deep-UV-light lithographic steps are repeatedly implemented like the way in IC industry. More details of this process are described in the Experimental Section.

on silicon), is grown on the designated regions by repeating the UV-exposure cycle. At this time, the first-layer SAM is regioselectively removed under the second piece of silicon hard mask. The ozone reacts with the added H_2O vapor to produce −OH, which can be modified on the broken molecule chain to form a new silanol surface. (VII) The Cr/Au metal layer is removed by wet etching. The mild metal etchants have been confirmed without a negative influence to the grown SAMs. (VIII) The microfluidic channels are closed by bonding with a previously molded transparent PDMS (polydimethylsiloxane) capping plate (see the Supporting Information 4). Purchased from Dow Corning, the Sylgard-184 PDMS is prepared with a weight ratio of 10:1 and precured at 80 °C for 1 h on a silicon mold wafer. According to various needs of surface functionalization in microchannels, the above-described process cycles can be flexibly designed.

Characterization with AFM, Contact-Angle, XPS, SIMS, and ATR-FTIR. AFM (atomic force microscopy) images were scanned in ambient atmosphere, with a Nanoscope V Multimode-8 AFM (Nano Surface Business, Bruker Corp., Santa Barbara, CA). All measurements were performed in peak-force mode at a scanning rate of 0.977 Hz with a resolution of 512 points per line. Static contact-angle (CA) measurement was carried out using an OCA15+ optical contact-angle meter purchased from Data Physics Inc. The used water drop is deionized water, and the oil drop is *N*-hexadecane. High-resolution XPS (X-ray photoelectron spectroscopy) data were obtained using an ESCALAB 250 system (Thermal VG Scientific Ltd.) equipped with an Al Kα monochromatic X-ray source (pass energy 20 eV, energy step size: 0.05 eV) and a double-focused concentric hemispherical analyzer. The sample surface was tilted at 58° with respect to the analyzer detector. The nominal pressure in the analysis chamber was lower than 2×10^{-10} mbar. Static SIMS (secondary-ion mass spectrometry) was performed with a SIMS Workstation (Hiden Analytical), which was equipped with both oxygen and cesium primary ion beams to allow sensitive detection of electropositive and electronegative elements, respectively. SIMS analysis was taken under 5 keV Cs primary ions at 45° while detecting positive and negative secondary ions. The employed beam is ∼100 pA. Analysis for each sample is repeated three times. An attenuation total reflection-Fourier transform infrared (ATR-FTIR) spectrometer (Vertex 70v, purchased from Bruker Inc.) was used for characterization of SAM. Spectra were recorded in the range of 1300−1400 cm^{-1} for the SAM of FAS-17 and ≡Si−OH-exposed silicon surface as well as in the range of 2800−3000 cm^{-1} for the SAM of OTS.

RESULTS AND DISCUSSION

Regioselective SAM Removal and Alternative Regrowth. Regioselective SAM removal is based on UV photochemical reaction.[20] Figure 2a schematically shows a process example where the existing SAM of FAS-17 is regioselectively removed and then replaced by another SAM of OTS. By repeating this process cycle, more kinds of SAMs can be sequentially constructed and patterned at designated segments of the microchannel. A typical microflow-chip nanoengineered with the above-mentioned processes is schematically shown in Figure 2b. The reason for the hard mask used for photolithography is because ozone needs to be locally generated under UV-light irradiation. Rather than a normal glass/quartz mask, the regioselectively hollowed hard mask facilitates inputting sufficient oxygen and water vapor through the patterned openings. Otherwise, if UV irradiation is operated in vacuum, a shorter wavelength of UV light will be required.[17] (see Supporting Information 8)

For building different surface properties at different micro-regions using the technique, the surface property covered by the formerly self-assembled SAM needs to be unchanged by the latter assembly of the second kind of SAM. To experimentally figure out the regular pattern, the most useful SAMs of FAS-17 (hydrophobic/oleophobic), OTS (hydrophobic/oleophilic), and PEG (hydrophilic/oleophilic) have been multiply grown on a silicon surface with various orders. From the surface contact-angle, AFM scanning, and ATR-FTIR combined characterization, the following conclusions have been made. A SAM with a relatively higher surface energy is difficult to be grafted on top of another SAM with lower surface energy. As long as the first grown SAM is dense enough, the surface will not obviously be influenced by the latter self-assembled SAM. OTS (with $-CH_3$ terminated) is with a surface energy of 24 mN/m higher than the $-CF_3$-terminated FAS-17 (14 mN/m)

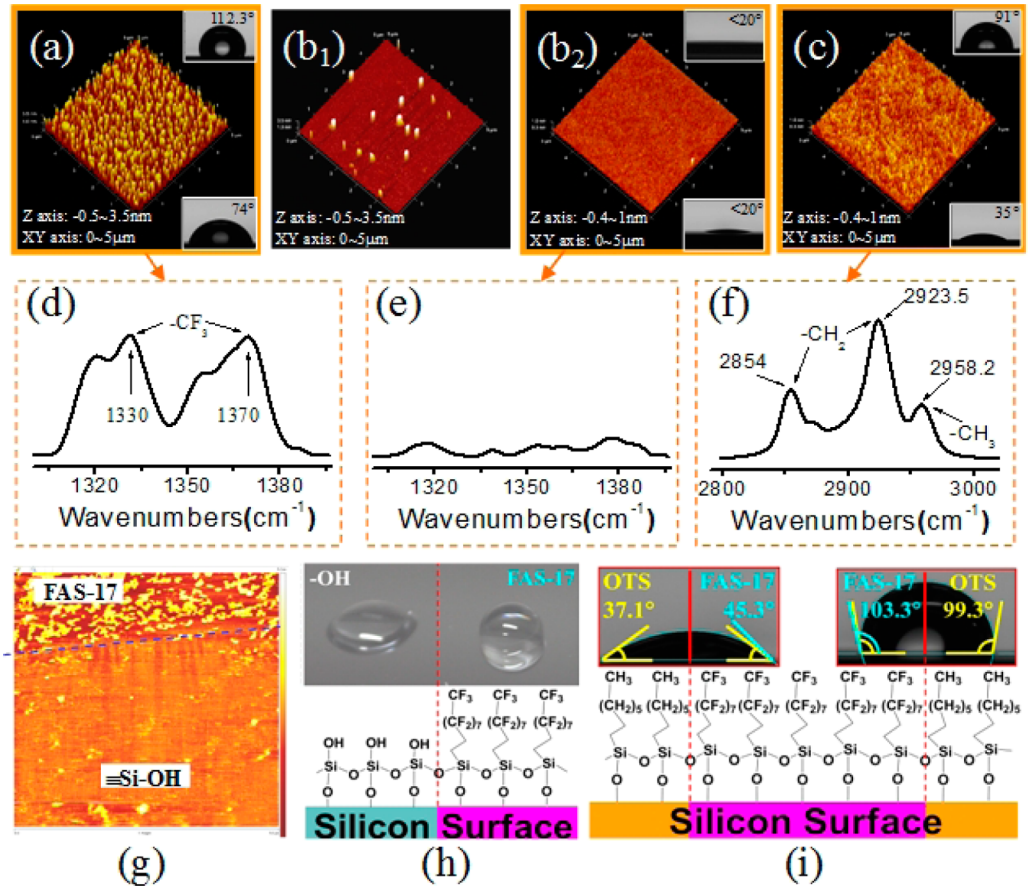

Figure 3. Characterization results of removing and regrowing SAM process and surface characterization of the border between different microregions. With ATR-FTIR spectrum, AFM scanning and contact-angle test, the process of FAS-17 SAM growth, removal, and OTS SAM regrowth on a silicon wafer is characterized. Peak-force mode AFM images and contact angles (with water drop at the top and oil drop at the bottom) sequentially show the surface situations: (a) after growth of hydrophobic/oleophobic FAS-17 SAM with high density and uniformity; (b_1) incomplete removal of the FAS-17 after deep-UV light exposure for 10 min; (b_2) thorough removal after UV illumination for 30 min (where the contact angles show a silanol-group-covered hydrophilic/oleophilic surface); (c) after regrowth of OTS SAM that changes the surface into hydrophobic but oleophilic, the surface-functionalized SAMs at the stages of a, b_2, and c are confirmed by the infrared spectra in d, e, and f, respectively. (d) Two peaks at 1330 and 1370 cm^{-1} demonstrate the existence of FAS-17 tail groups. Note: The FTIR spectra in d and e possess the same magnification in *Y*-axis unit for comparison. (f) OTS is characterized by the three peaks that are the symmetric 2854 cm^{-1} and asymmetric 2923.5 cm^{-1} stretching modes of $-CH_2-$ as well as the contribution at 2958.2 cm^{-1} from the asymmetric stretch in the $-CH_3$ terminal group. (g) Peak-force AFM image (scanning area = 5 μm × 5 μm) showing the surface topography across the border between the FAS-17 and the −OH-covered regions. (h) Two water drops located at the hydrophilic (left) and hydrophobic (right) regions show disparity in the drop shape. (i) An oil drop stands cross the left OTS/FAS-17 boundary and a water-drop stands across the right FAS-17/OTS boundary. Difference between the left and the right contact angles is observed in each drop.

but lower than the −OH-terminated PEG (63 mN/m).[22] In multiple self-assemblies, the first grown molecule layer would be FAS-17. Then OTS and PEG follow behind (see Supporting Information 5).

Characterization Results. Regioselective surface modification of multiple SAMs has been characterized by AFM scanning, contact-angle test, and ATR-FTIR (attenuation total reflection-Fourier transform infrared) spectrum. AFM surface-scanning images shown in Figure 3a−c correspond to the process stages given in Figure 2a: (a) the SiO_2 surface covered by FAS-17; (b1 and b2) the surface at the moment when FAS-17 is partly removed by UV illumination (at 100 °C for 10 min) and the clean surface with the SAM entirely removed by 30 min exposure, respectively; (c) the surface of the same region covered by the regrown OTS. Surface wetting properties are characterized by testing the contact angles of water drop (shown at the top inset of each AFM image) and oil drop (*N*-hexadecane, at each bottom inset). This contact-angle test is implemented at the process stages of FAS-17 being modified, ≡Si−OH being recovered after removal of FAS-17 and OTS being regrown at the same microregion. The water/oil angles of 113°/74°, <20°/<20°, and 91°/35° well confirm the designated hydrophobic/oleophobic, hydrophilic/oleophilic, and hydrophobic/oleophilic surface wetting properties. The nanofunctionalized surface is also confirmed by the corresponding FTIR spectra shown in Figure 3d−f. In contrast with the FAS-17-removed surface that is characterized in Figure 3e, the two peaks at 1330 and 1370 cm^{-1} observed in Figure 3d are assigned to $-CF_3$ asymmetric stretches of FAS-17. The spectrum in Figure 3f verifies the existence of the regrown OTS, where the C−H stretch is identified by the three peaks: the symmetric 2854 cm^{-1} and asymmetric 2923.5 cm^{-1} stretching modes of $-CH_2-$ as well as the peak at 2958.2 cm^{-1} for the asymmetric stretch in $-CH_3$.

The AFM scanning image of Figure 3g shows the boundary between the adjacent areas covered by FAS-17 and −OH,

respectively. To further identify the border microregion, two water drops located at the double sides of the borderline are shown in Figure 3h. Great disparity in contact angle is observed that indicates a surface-wetting difference between the hydrophobic and the hydrophilic areas. The results also imply that the UV-photolighgraphy patterned hydrophobic/hydrophilic boundary line is quite sharp. A more interesting phenomenon can be observed in Figure 3i, where the central area is modified with FAS-17 but its double sides are both covered by the regrown OTS. By placing the oil (*N*-hexadecane) drop across the left borderline, different contact angles are tested as 37.1° at the left side and 45.3° at the right side. Similarly, the water drop across the right border also shows disparity in the double-side angles that are 103.3° at left and 99.3° at right. The results make clear distinction to the boundary between the more hydrophobic FAS-17 microregion and the more oleophilic OTS one. XPS and SIMS characterization results can be found in Supporting Information 6,7.

Surface-Directed Flow Guide by Regioselective Multi-SAMs. A micromachined three-branch manifold microchip is designed with the schematic shown in Figure 4, where the three branches are modified with FAS-17 SAM, OTS SAM, and ≡Si−OH group for individual functionalization of the desired flow-guide surface. On the basis of fluidic knowledge, when fluid just flows into a microchannel (i.e., the channel has not been completely filled with the fluid), the flowing direction depends on the capillary pressure at the liquid/gas interface.[2] When the liquid flows to the three-way manifold it prefers to flow into the branch which provides larger capillary pressure (see Supporting Information 1).

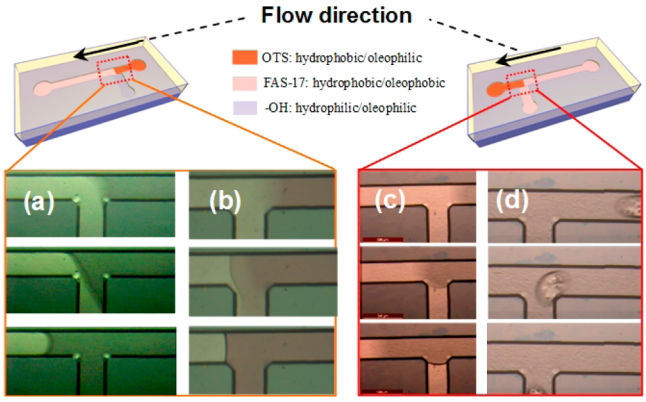

Figure 4. Expetimentally obtained surface-directed flow-guide phenomena. Different SAMs are regioselectively modified at different branches. (a) Oil fluid front prefers to flow toward the more oleophilic branch. (b) Water fluid front turns to flow into the hydrophilic branch. (c) Oil front is surface directed and pumped into the oleophilic branch. (d) After water continually flows into the two branches, a macrosized oil bubble (mixed in the water flow) prefers to turn into a less oleophilic branch due to less resistive force at the oleophobic surface.

In comparison of capillary pressure between two branches, only the contribution from the advancing contact angle of θ_{Si} needs to be taken into account, since the pressure difference comes only from the differently modified silicon surface at the different branches. The contribution from the nonmodified PDMS surface (at the cap plate of the channel) to the pressure is always the same for each branch and, thus, can be ignored.

According to the calculated pressure-drop results, water should prefer to flow into the −OH-modified branch instead of the FAS-17 one due to the great capillary-pressure difference of 267 N/m^2. Similarly, oil prefers to flow into the OTS or −OH-modified branch rather than the FAS-17 one, due to the capillary-pressure difference of 40 N/m^2 or larger than 50 N/m^2, respectively. The reasonable speculation has been confirmed by the microfluidic experiment shown in Figure 4. When the fluid front reaches the branching point of the manifold, as shown in Figure 4a and 4b, either oil or water automatically turns into the −OH-covered oleo(hydro)philic branch rather than directly entering the FAS-17-modified oleo(hydro)phobic one. As for flow-direction choice between the OTS-modified branch and the FAS-17 one, Figure 4c shows that the oil flow front directly enters the oleophilic former instead of the oleophobic latter.

When the fluid has already filled the microchannel, however, the surface-guided flow phenomena are different from the above-mentioned fluid-front case. Selection of the continuing-flow direction at the branching point obeys by the rule of resistive force minimization, e.g., water (or oil) prefers to flow along the more hydrophobic branch (or the more oleophobic one). After water has continually flown in both the hydrophobic turning branch (modified with FAS-17) and the hydrophobic straight branch (modified with OTS), we mix big-sized oil bubbles in the water flow. It is observed in Figure 4d that all the oil bubbles turn into the oleophobic turning branch instead of the oleophlic straight branch. Herein the big-sized oil bubble has physically touched the bottom surface of the channel and, obviously, the bubbles prefer to go through the way with lower resistive force,[23−25] i.e., the oleophobic FAS-17 branch with lower friction force.

Patterned Multi-SAMs for Oil/Water Mixing and Liquid-Phase Extraction. Mixing and chemical extraction between mutually immiscible oil and water in a microchannel is indeed difficult. However, such oil/water mixing and extraction is frequently required in the fields of agriculture investigation, food-safety detection, and biochemical analysis. When oil and water are introduced into a conventional microchannel they prefer to remain as two-phase laminar flow. This has been confirmed by not only our experiment (detailed in Supporting Information 2) but also fluidic dynamics calculation.[26] Only with molecule diffusion at the flow interface the channel length Z required for full extraction can be defined as $Z = U(w/2)^2D^{-1}$,[27] where w is the channel width, U is the flow rate, and D is the extraction diffusivity. For extracting methylene blue from oil of CH_2Cl_2 to water the D value is quite low and merely at the level of 10^{-9} m^2/s.[28] According to the flow rate of U = 0.5 m/s used in our experiment, the full extraction required channel length of Z would be at least 11 m, which is impossible for a microchannel system. In other words, oil-to-water extraction in a conventional microchannel will result in a low efficiency due to the fact that the extraction only occurs at the laminar flow interface.

Many efforts on passive micromixers have been made to either increase the contact area by separation/recombination or form chaotic-flow convection by fabricating complex 3D winding channels.[29,30] Compared with those active mixing devices,[31−35] passive micromixers do not require external power but often need larger chip size or complicated fabrication to integrate 3D structures in the microchannel.[36] Stirring the stream into chaotic advection is expected to be a promising solution for more efficient micromixing at low Reynolds

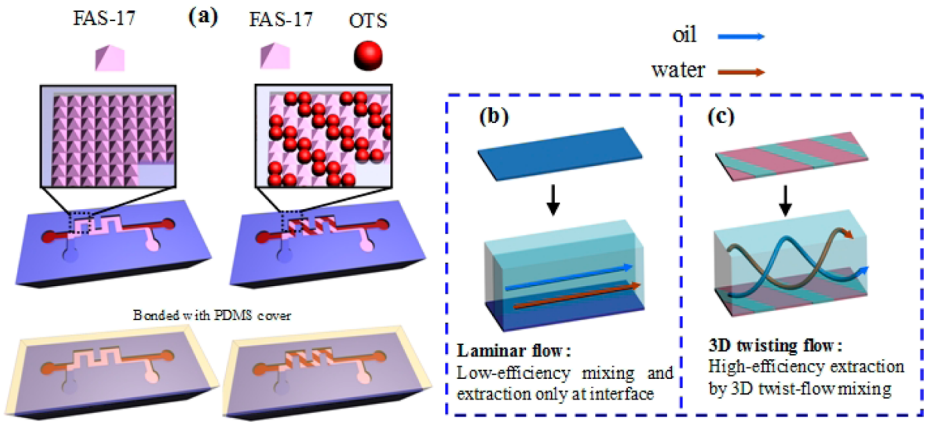

Figure 5. Comparison of microchannel chips with different nanosurface. (a) Comparison in surface construction between two kinds of microchannel chips for liquid–liquid mixing and extraction. At the surface of the serpentine mixer the conventional chip is uniformly modified with oleophobic FAS-17, while the surface-direct chip is modified with the oleophobic/oleophilic "dual-color" stripe array. Besides, oleophilic OTS is modified at the oil inlet/outlet, while a hydrophilic ≡Si−OH surface with high capillary force and a hydrophobic FAS-17 surface with low flow resistance are formed at the water inlet and outlet, respectively. (b) Schematic of the low-efficiency mixing/extracting oil/water two-phase laminar flow in the conventional channel due to isotropic flow resistance from the single SAM modified surface. (c) Schematic of high-efficiency mixing/extracting 3D helical flow due to the oleophobic/oleophilic mutual-spaced stripe array that is surface directed with anisotropic flow resistance of the inclined "dual-color" SAMs (see Supporting Information 3).

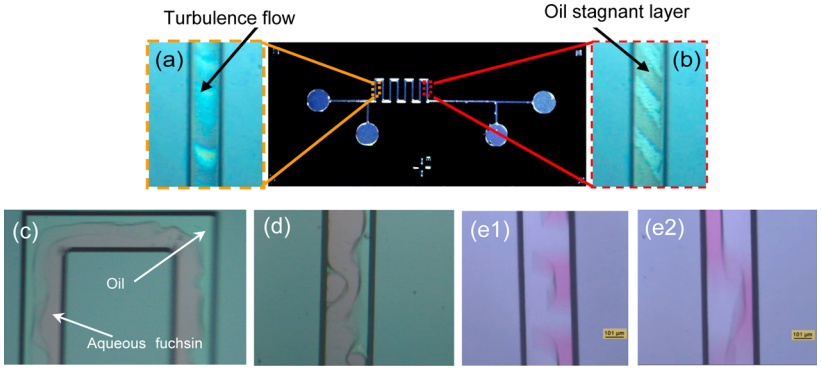

Figure 6. Experimental observation of oil (CH_2Cl_2) turbulence flow induced by the "two-tone" surface modification in the micromixing channel. The typical twist-flow pattern of the oil flow is shown in a. After the oil fluid is driven out by air, the stripe-array nanopattern is visualized by the oil stagnant layer on top of the OTS strips, which is shown in b. Then, water/oil mixing phenomena are experimentally observed in the "two-tone" modified microchannel. Pink-colored fuchsin water solution is herein used as the aqueous phase and *n*-hexane as the oil phase. (c) At 80 μL/min flow rate for both the oil and the water, the two fluidic phases begin to get into each other's region. (d) When the flow rate is increased to 110 μL/min, the water stream starts to wind. When the flow rate is further increased to 170 μL/min, both folding (e1) and rotation (e2) of the water stream can be observed.

number. By employing the multi-SAMs patterning technology, 3D twisting flow is anticipated to be passively generated for efficient mixing/extraction in a simple pressure-driven microchannel.

The idea is to pattern multi-SAMs at the channel surface to guide the flow into 3D turbulence, thereby realizing high-efficiency oil/water mixing. Sketched in Figure 5a is the designed oil-to-water extraction microchannel chip that consists of a passive micromixer, two inlets, and two outlets for oil/water separation. In addition to the multi-SAM modifications at the inlets/outlets for designated liquid I/O and postextraction separation between oil and water, the surface of the serpentine microchannel mixer is modified into a pattern of 45°-inclined FAS-17/OTS alternate stripe array. The arrayed dual-SAM "two-tone" stripe is designed to be 150 μm in width. Another traditional chip with an identical mixer structure is also fabricated for experimental comparison, where the mixing region is surface modified only with FAS-17. The oil/water flow in the traditional mixer is expected to be still two-phase laminar flow, as schematically shown in Figure 5b. In contrast, chaotic flow[27] is expected to occur in the "dual-color" striped channel, where the two inversely wetting surfaces of oleophilic OTS and oleophobic FAS-17 are mutually spaced for generating 3D twist flow. When oil continually flows onto the FAS-17-covered stripe surface it prefers to fast slip onto the next OTS stripe where the oil tends to adhere to form a stagnant layer. On the basis of the heterogeneous surface-directing properties, the oil fuild undergoes less flow resistance on every FAS-17 strips and is guided to follow the FAS-17 stripe every time when it reaches the OTS/FAS-17 boundary. The experimental phenomenon in Figure 4d has indirectly verified this point. As is vividly illustrated in Figure 5c, the oil will follow a helical trajectory to form 3D chaotic flow.[27,37] Relatively, the effect of the stripe pattern on water flow is much weaker, as both SAMs are hydrophobic. When the fluid of water is added into the 3D helical oil flow, the strong stirring effect will significantly enhance the oil/water mixture. The designed diagonal stripes promote convection in the transverse direction and increase the

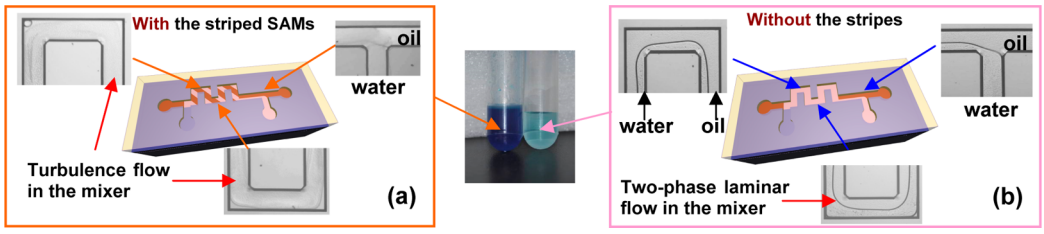

Figure 7. Experimental observation at the serpentine micromixer and comparison in mixing/extraction performance. (a) In the "two-tone" striped chip, a fast mixture of the oil/water flow at the serpentine mixer and the after-extraction separation at the outlets are observed. (b) In the traditional chip without the flow-guiding SAMs, two-phase laminar flow remains throughout the mixer and the outlets. By comparison between the two extractants collected in the two tubes (see the center of the figure), apparently the oil-to-water extracted methylene blue from the surface-striped mixer is a much darker color than that extracted from the traditional mixer.

oil/water contact area, thereby speeding up the process of mixing and extraction.

The effect of the modified "two-tone" stripes on the mixing microchannel is experimentally validated. First, the oil of CH_2Cl_2 is flown into the "two-tone" striped mixer. Twisting oil flow is clearly observed in the micrograph of Figure 6a. In Figure 6b the patterned stripes are clearly visualized at the moment when the oil just flows out the channel and the residual oil stagnant layer is still adhered on the surface of OTS. Then, the oil of *n*-hexane and water are both introduced into the mixing channel to examine generation of twist flow in the two-phase fluidic channel. For easy observation, pink-colored fuchsin aqueous solution is used as the water phase. In the channel of 300 μm width, each phase begins to get into each other's side when the flow rate is increased to 80 μL/min. With the flow rate is 110 μL/min, the water phase starts to take a winding shape. Finally, folding and rotating of the water stream are both observed at the further increased flow rate of 170 μL/min. The upper limit of the flow rate for the 300 μm wide mixing channel is experimentally obtained as about 240 μL/min, which is mainly determined by the oil/water separation after extraction. As shown in Figure 5a, the channel segment near the outletting T-joint is side-by-side modified by the two SAMs. A too high flow rate will cause incomplete oil/water separation (see Supporting Information 9).

In general, there have been two effective methods to improve the liquid–liquid mixing and extraction performance by either increasing the surface-to-bulk ratio or decreasing the diffusion path. In the laminar flow extraction study reported by Priest et al.,[38] the surface-to-bulk ratio was given as about 15000 m^{-1}, which is equivalent to the surface-to-bulk ratio of a droplet with a diameter of 400 μm. Such a droplet is too large to be accommodated in our microchannel. In other words, the surface-to-bulk ratio of laminar flow is far from big enough to meet our microfluidic requirement. On the other hand, generating droplets[39] is indeed an elegant method for increasing the surface-to-bulk ratio. Actually, as observed in our extraction experiment, the generated water droplets can extend, fold, and rotate in the channel, thereby achieving better extraction performance. Our turbulence flow provides both high a surface-to-bulk ratio and a short diffusion path.

In order to visualize the experimental chemical-extraction results, colorful methylene blue is previously dissolved into an oil of dichloromethane (CH_2Cl_2) for the oil-to-water extraction experiment. With or without the "two-tone" striped multi-SAMs, two identically microstructured chips are used for the same extraction experiment. For the chip with the "dual-color" stripes, Figure 7a shows quick disappearance of the oil/water interface that indicates sufficient mixing. With the high-efficiency mixing, the methylene blue can be extracted into water by higher solubility. Through the postextraction channel segment, which is deliberately modified into the half and half straight-line pattern shown in Figure 5a, the water can be gradually separated from the oil and drained out from its own outlet. In the conventional chip shown in Figure 7b, the two-phase laminar flow can be observed throughout the whole serpentine mixer, indicating poor mixing/extracting consequently. The two extracted methylene-blue samples are compared at the central part of Figure 7. The obviously deeper blue water from the "dual-color" striped microextraction chip validates the effect of the regioselectively integrated multi-SAMs on the surface-directed flow-guide function.

To investigate the influence of the channel geometry to the efficiency of the MB extraction from oil to water, we designed and fabricated five types of the "two-tone" modified mixing/extraction microchips with varied channel geometries. From the highest extracted MB concentrations of 1.12 μM, which is obtained from the no. 4 chip, the highest extraction rate of about 93% is achieved. More details about the influence of the channel geometry to extraction performance can be seen in Supporting Information 10.

CONCLUSIONS

We demonstrated a batch fabrication method to regioselectively integrate multiple (three or more) silane-SAMs in silicon microfluidic chips. To achieve uniform surface modification, the SAMs are vapor-phase deposited on an open microfluidic channel (i.e., before the channel is closed by bonding). With the commercial MVD machine that is equipped with a good surface pretreatment tool, a vacuum conditioner, and a precise flow controller, the quality of the vapor-phase surface modification is much better than conventional liquid-phase SAM modification. With the help of the hollow mask, UV irradiation for patterning SAMs can be realized in a short period of time. The "selective SAM removal and alternative SAM regrowth" process cycle can be repeated to batch fabricate patterned multi-SAMs at the surface of fluidic channels for surface-directed flow-guide functions. The surface-guiding effect of the patterned multi-SAMs on functional microchannel flow has been experimentally demonstrated. By modifying arrayed oleophobic/oleophilic "dual-color" SAM stripes on the surface of a micromixer, 3D twist-flow enhanced oil/water passive mixture and high-efficiency liquid-phase extraction are realized. The developed technique in this study is promising for wide applications of microfluidic systems.

■ ASSOCIATED CONTENT

Supporting Information

Capillary-pressure calculation, experiment of oil/water two-phase laminar flow in the microchannel without the "dual-color" multi-SAM stripes, the micromixer chip fluidics with the "two-tone" multi-SAM stripes, PDMS/Si microchannel bonding process, the influence of deposition sequence of SAMs to surface wetting property, XPS and SIMS characterization of SAMs, variation of water contact angles with the time of UV light irradiation, the influence of the microchannel geometries, and the flow rate to the microfluidics. This material is available free of charge via the Internet at http://pubs.acs.org.

■ AUTHOR INFORMATION

Corresponding Author

*E-mail: xxli@mail.sim.ac.cn.

Author Contributions

‡C.C. performed the microchip design, fabrication, experiments, and measurement. P.X. designed the SAMs and performed the characterization. X.L. contributed to the idea and performed the analysis. C.C. and X.L. wrote the manuscript.

Notes

The authors declare no competing financial interest.

■ ACKNOWLEDGMENTS

The research was supported by NSF of China (91323304, 91023046, 61021064) and Chinese 973 Project (2011CB309503). The authors thank Dr. Helena Stec and Dr. Graham Cooke for help with SIMS characterization.

■ ABBREVIATIONS

SAMs, self-assembled monolayers; IC, integrated circuit; UV, ultraviolet; μ-TAS, micrototal analysis system; MVD, molecule-vaporized deposition; FAS-17, heptadecafluorodecyl-trimethoxysilane; OTS, octyltrichlorosilane; PEG, 2-[methoxy-(polyethyleneoxy)propyl]trimethoxysilane; AFM, atomic force microscopy; ATR-FTIR, attenuation total reflection-Fourier transform infrared; PDMS, polydimethylsiloxane; XPS, X-ray photoelectron spectroscopy; SIMS, secondary-ion mass spectrometry

■ REFERENCES

(1) Yasui, T.; Omoto, Y.; Osato, K.; Kaji, N.; Suzuki, N.; Naito, T.; Watanabe, M.; Okamoto, Y.; Tokeshi, M.; Shamotoc, E.; Babaabd, Y. Microfluidic Baker's Transformation Device for Three-dimensional Rapid Mixing. *Lab Chip* **2011**, *11*, 3356−3360.

(2) Zhao, B.; Moore, J. S.; Beebe, D. J. Surface-Directed Liquid Flow Inside Microchannels. *Science* **2001**, *291*, 1023−1026.

(3) Iqbal, P.; Rawson, F. J.; Ho, W.; Lee, S. F.; Leung, K. C. F.; Wang, X.; Beri, A.; Preece, J. A.; Ma, J.; Mendes, P. M. Surface Molecular Tailoring Using pH-Switchable Supramolecular Dendron-Ligand Assemblies. *ACS Appl. Mater. Interfaces* **2014**, *6*, 6264−6274.

(4) Ellinas, K.; Pujari, S. P.; Dragatogiannis, D. A.; Charitidis, C. A.; Tserepi, A.; Zuilhof, H.; Gogolides, E. Plasma Micro-nanotextured, Scratch, Water and Hexadecane Resistant, Superhydrophobic, and Superamphiphobic Polymeric Surfaces with Perfluorinated Monolayers. *ACS Appl. Mater. Interfaces* **2014**, *6*, 6510−6524.

(5) Hudalla, G. A.; Murphy, W. L. Using "Click" Chemistry to Prepare SAM Substrates to Study Stem Cell Adhesion. *Langmuir* **2009**, *25*, 5737−5746.

(6) Schmitt, S. K.; Murphy, W. L.; Gopalan, P. Crosslinked PEG Mats for Peptide Immobilization and Stem Cell Adhesion. *J. Mater. Chem. B* **2013**, *1*, 1349−1360.

(7) Dawood, M. K.; Zheng, H.; Liew, T. H.; Leong, K. C.; Foo, Y. L.; Rajagopalan, R.; Khan, S. A.; Choi, W. K. Mimicking Both Petal and Lotus Effects on a Single Silicon Substrate by Tuning the Wettability of Nanostructured Surfaces. *Langmuir* **2011**, *27*, 4126−4133.

(8) Alagta, A.; Felhosi, I.; Bertoti, I.; Kalman, E. Corrosion Protection Properties of Hydroxamic Acid Self-Assembled Monolayer on Carbon Steel. *Corros. Sci.* **2008**, *50*, 1644−1649.

(9) Irving, D. L.; Brenner, D. W. Diffusion on a Self-Assembled Monolayer: Molecular Modeling of a Bound Plus Mobile Lubricant. *J. Phys. Chem. B* **2006**, *110*, 15426−15431.

(10) Yokota, K.; Takai, K.; Enoki, T. Carrier Control of Graphene Driven by the Proximity Effect of Functionalized Self-Assembled Monolayers. *Nano Lett.* **2011**, *11*, 3669−3675.

(11) Xu, P. C.; Li, X. X.; Yu, H. T.; Liu, M.; Li, J. G. Self-Assembly and Sensing-Group Graft of Pre-modified CNTs on Resonant Micro-Cantilevers for Specific Detection of Volatile Organic Compound Vapors. *J. Micromech. Microeng.* **2010**, *20*, 115003.

(12) Chen, Y.; Xu, P. C.; Li, X. X. Self-Assembling Siloxane Bilayer Directly on SiO_2 Surface of Micro-Cantilevers for Long-Term Highly Repeatable Sensing to Trace Explosives. *Nanotechnology* **2010**, *21*, 265501.

(13) Logtenberg, H.; Lopez-Martinez, M. J.; Feringa, B. L.; Browne, W. R.; Verpoorte, E. Multiple Flow Profiles for Two-phase Flow in Single Microfluidic Channels through Site-selective Channel Coating. *Lab Chip* **2011**, *11*, 2030−2034.

(14) Arayanarakool, R.; Shui, L.; Van De Berg, A.; Eijkel, J. C. T. A New Method of UV-patternable Hydrophobization of Micro- and Nanofluidic Networks. *Lab Chip* **2011**, *11*, 4260−4266.

(15) Derzsi, L.; Jankowski, P.; Lisowski, W.; Garstecki, P. Hydrophilic Polycarbonate for Generation of Oil in Water Emulsions in Microfluidic Devices. *Lab Chip* **2011**, *11*, 1151−1156.

(16) Bounds, C.; Upadhyay, J.; Totaro, N.; Thakuri, S.; Garber, L.; Vincent, M.; Huang, Z.; Hupert, M.; Pojman, J. Fabrication and Characterization of Stable Hydrophilic Microfluidic Devices Prepared via the in Situ Tertiary-Amine Catalyzed Michael Addition of Multifunctional Thiols to Multifunctional Acrylates. *ACS Appl. Mater. Interfaces* **2013**, *5*, 1648−1655.

(17) Shirai, K.; Mawatari, K.; Kitamori, T. Extended Nano fluidic Immunochemical Reaction with Femtoliter Sample Volumes. *Small* **2014**, *10*, 1514−1522.

(18) Whitesides, G. M. The Origins and the Future of Microfluidics. *Nature* **2006**, *442*, 368−373.

(19) Squires, T. M.; Quake, S. R. Microfluidics: Fluid Physics at the Nanoliter Scale. *Rev. Mod. Phys.* **2005**, *77*, 977−1026.

(20) Herzer, N.; Hoeppener, S.; Schubert, U. S. Fabrication of Patterned Silane Based Self-assembled Monolayers by Photolithography and Surface Reactions on Silicon-Oxide Substrates. *Chem. Commun.* **2010**, *46*, 5634−5652.

(21) Ravenscroft, M. S.; Bateman, K. E.; Shaffer, K. M.; Schessler, H. M.; Jung, D. R.; Schneider, T. W.; Montgomery, C. B.; Custer, T. L.; Schaffner, A. E.; Liu, Q. Y.; Li, Y. X.; Barker, J. L.; Hickman, J. J. Developmental Neurobiology Implications from Fabrication and Analysis of Hippocampal Neuronal Networks on Patterned Silane-Modified Surfaces. *J. Am. Chem. Soc.* **1998**, *120*, 12169−12177.

(22) Janssen, D.; De Palma, R.; Verlaak, S.; Heremans, P.; Dehaen, W. Static Solvent Contact Angle Measurements, Surface Free Energy and Wettability Determination of Various Self-Assembled Monolayers on Silicon Dioxide. *Thin Solid Films* **2006**, *515*, 1433−1438.

(23) Ishida, N.; Inoue, T.; Miyahara, M.; Higashitani, K. Nano Bubbles on a Hydrophobic Surface in Water Observed by Tapping-Mode Atomic Force Microscopy. *Langmuir* **2000**, *16*, 6377−6380.

(24) Lou, S. T.; Ouyang, Z. Q.; Zhang, Y.; Li, X. J.; Hu, J.; Li, M. Q.; Yang, F. J. Nanobubbles on Solid Surface Imaged by Atomic Force Microscopy. *J. Vac. Sci. Technol. B* **2000**, *18*, 2573−2575.

(25) Yang, J. W.; Duan, J. M.; Fornasiero, D.; Ralston, J. Very Small Bubble Formation at the Solid-Water Interface. *J. Phys. Chem. B* **2003**, *107*, 6139−6147.

(26) Reynolds, O. An Experimental Investigation of the Circumstances Which Determine Whether the Motion of Water Shall Be

Direct or Sinuous, and of the Law of Resistance in Parallel Channels. *Philos. Trans. R. Soc. London* **1883**, *174*, 935−982.
(27) Stroock, A. D.; Dertinger, S. K. W.; Ajdari, A.; Mezic, I.; Stone, H. A.; Whitesides, G. M. Chaotic Mixer for Microchannels. *Science* **2002**, *295*, 647−651.
(28) Leaist, D. G. The Effects of Aggregation, Counterion Binding, and Added Nacl on Diffusion of Aqueous Methylene-Blue. *Can. J. Chem.-Rev. Can. Chim.* **1988**, *66*, 2452−2457.
(29) Koch, M.; Chatelain, D.; Evans, A. G. R.; Brunnschweiler, A. Two Simple Micromixers Based on Silicon. *J. Micromech. Microeng.* **1998**, *8*, 123−126.
(30) Liu, R. H.; Stremler, M. A.; Sharp, K. V.; Olsen, M. G.; Santiago, J. G.; Adrian, R. J.; Aref, H.; Beebe, D. J. Passive Mixing in a Three-Dimensional Serpentine Microchannel. *J. Microelectromechan. Syst.* **2000**, *9*, 190−197.
(31) Luong, T. D.; Phan, V. N.; Nguyen, N. T. High-Throughput Micromixers Based on Acoustic Streaming Induced by Surface Acoustic Wave. *Microfluid. Nanofluid.* **2011**, *10*, 619−625.
(32) Ahmed, D.; Mao, X. L.; Juluri, B. K.; Huang, T. J. A Fast Microfluidic Mixer Based on Acoustically Driven Sidewall-Trapped Microbubbles. *Microfluid. Nanofluid.* **2009**, *7*, 727−731.
(33) Lim, C. Y.; Lam, Y. C.; Yang, C. Mixing Enhancement in Microfluidic Channel with a Constriction under Periodic Electro-Osmotic Flow. *Biomicrofluidics* **2010**, *4*, 14101.
(34) Wang, Y.; Zhe, J.; Chung, B. T. F.; Dutta, P. A Rapid Magnetic Particle Driven Micromixer. *Microfluid. Nanofluid.* **2008**, *4*, 375−389.
(35) Bockelmann, H.; Heuveline, V.; Barz, D. P. J. Optimization of an Electrokinetic Mixer for Microfluidic Applications. *Biomicrofluidics* **2012**, *6*, 024123.
(36) Fang, Q.; Kim, D. P.; Li, X.; Yoon, T. H.; Li, Y. Facile Fabrication of a Rigid and Chemically Resistant Micromixer System from Photocurable Inorganic Polymer by Static Liquid Photolithography (SLP). *Lab Chip* **2011**, *11*, 2779−2784.
(37) Hsieh, S. S.; Chen, J. H.; Su, G. C. Visualization and Quantification of Chaotic Mixing for Helical-Type Micromixers. *Colloid Polym. Sci.* **2012**, *290*, 1547−1559.
(38) Priest, C.; Zhou, J. F.; Klink, S.; Sedev, R.; Ralston, J. Microfluidic Solvent Extraction of Metal Ions and Complexes from Leach Solutions Containing Nanoparticles. *Chem. Eng. Technol.* **2012**, *35*, 1312−1319.
(39) Mary, P.; Studer, V.; Tabeling, P. Microfluidic Droplet-Based Liquid-Liquid Extraction. *Anal. Chem.* **2008**, *80*, 2680−2687.